Proceedings of the 10th Brazilian Congress of Thermal Sciences and Engineering – ENCIT 2004
Braz. Soc. of Mechanical Sciences and Engineering – ABCM, Rio de Janeiro, Brazil, Nov. 29 – Dec. 03, 2004

Paper CIT04-0515

Statistical Properties of Boundary Layers Subject to Changes in Surface Roughness

Wagner M. Brasil
Mechanical Engineering Program (PEM/COPPE/UFRJ)
C.P. 68503, 21945-970, Rio de Janeiro, Brazil
e-mail wbrasil@mecanica.coppe.ufrj.br

Su Jian
Nuclear Engineering Program (PEN/COPPE/UFRJ)
C.P. 68509, 21945-970, Rio de Janeiro, Brazil
e-mail sujian@lmn.coppe.ufrj

Atila P. Silva Freire
Mechanical Engineering Program (PEM/COPPE/UFRJ)
C.P. 68503, 21945-970, Rio de Janeiro, Brazil
e-mail atila@mecanica.coppe.ufrj.br

Abstract. ***This work discusses the statistical properties of a turbulent flow that is made to past from a rough to a smooth surface. The interest is on assessing the behaviour of the error in origin as well as of the roughness function. The work, in addition, discusses some relevant turbulent scales of the flow, the energy spectra, the second- and third-order moments and the shape factor.***

keywords: *Statistical properties, turbulence, boundary layer, roughness, thermal-anemometry.*

1. Introduction

The structure of turbulence in flows over rough surfaces has been the subject of considerable research, in particular, in the last twenty years. While most of the works prior to the nineties focused on investigations of the mean properties of the flow, a shift to a deeper understanding of other statistical properties of the flow has been recently observed (Ligrani and Moffat (1985), Perry et al. (1987), Bandyopadhyay (1987), Bandyopadhyay and Watson (1988), Krogstad and Antonia (1994)).

In fact, Avelino and Silva Freire (2002) and Loureiro and Silva Freire (2004) have shown that much remains to be understood about turbulent flows over rough surfaces even in what concerns some of their mean properties. That certainly is the case for the error in origin, which has been thoroughly investigated in those two publications.

In this work, we will strive to disclose some of the statistical properties of a boundary layer subject to a rough-to-smooth step change in surface condition. This flow is of particular interest due to the slow recovery in properties following the change. In this situation, the rough-wall flow dominates the rate of diffusion of the disturbances for a considerable length, dictating conditions that are far from self-preserving (Antonia and Luxton (1971), Antonia and Luxton (1972), Antonia et al. (1977)).

The present work aims specifically at assessing the effects of the rough-to-smooth step change in surface on the error in origin and on the roughness function. It is a fact that the recent development on computational fluid dynamics has placed a strong emphasis on the accurate measurement of mean velocity components and of Reynolds stresses. However, the fundamental statistical approach to turbulence analysis still plays a central role in the understanding of complex flows. Thus, the present work will also discuss some relevant turbulent scales of the flow, the energy spectra, the second- and third-order moments and the shape factor.

The chief measuring technique to be employed here will be the hot-wire anemometry. A hot-wire anemometer is a low cost equipment with a very high frequency response, relative small size, low noise levels, high accuracy and a continuous analog signal. For this reason, there is no surprise such equipments are judged ideal for measurements in low and moderate turbulence intensity flows.

2. The one-dimensional spectrum

The three-dimensional energy spectrum is one of the key concepts in turbulence theory (Tennekes and Lumley (1972)). However, in the laboratory, researchers find it much more convenient to measure the longitudinal

spectrum. This, of course, sets the problem of relating the measured one-dimensional spectrum to the theoretical three-dimensional spectrum.

If an one dimensional flow has its movement captured by a hot-wire anemometer, the velocity fluctuations may be decomposed into their harmonic components with respect to the angular frequency, ω. Then, by analyzing and averaging the signal, the resulting frequency spectrum, $E_{11}(\omega)$ must have the property

$$\left\langle u_1'^{\,2} \right\rangle = \int_0^\infty E_{11}(\omega) d\omega. \tag{1}$$

To relate the frequency and wavenumber spectra, the common practice is to use the 'frozen convection' hypothesis of Taylor that considers the changes in u_1 with time at a fixed point to be due to the passage of a frozen pattern of turbulent motion.

This is equivalent to state

$$u(x,t) = u(x - \overline{u_1}t, 0), \tag{2}$$

or else,

$$\frac{\partial}{\partial t} = -\overline{u_1}\frac{\partial}{\partial x_1}. \tag{3}$$

The Taylor hypothesis is open to scrutiny even today, but it is at least a very good approximation and hence will be used extensively here.

Defining

$$E_{11}(k_1) = \overline{u_1} E_{11}(\omega), \quad k_1 = \omega/\overline{u_1}. \tag{4}$$

Then, it follows that

$$\int_0^\infty E_{11}(\omega) d\omega = \int_0^\infty \frac{E_{11}(k_1) d\omega}{\overline{u_1}} = \int_0^\infty E_{11}(k_1) dk_1 = \left\langle u_1'^{\,2} \right\rangle. \tag{5}$$

An extension of the above equation to three dimensions is trivial, it suffices to integrate out the dependence of $E_{11}(k_1)$ on k_2 and k_3 to obtain

$$E(k) = \frac{k^3 d[k^{-1} dE_{11}(k)/dk]}{dk}. \tag{6}$$

3. Time domain analysis

The output signal of a hot-wire anemometer is random by its very nature (Bruun (1995)). Therefore, a statistical description of its contents is in order. Next we will very briefly remind the reader some of the basic concepts in random data analysis and introduce the paper notation.

The autocorrelation function for the flow velocity is denoted by R_u, the autocorrelation coefficient function by ρ_u and the auto-spectral density function by S_u.

Consider a time-history velocity record, u. It can be split into a mean, $\overline{u}$ and a fluctuating component, u',through

$$u(t) = \overline{u} - u' \tag{7}$$

where the mean value is the average of all values, defined by

$$\overline{u} = lim_{T\to\infty} \frac{1}{T} \int_0^T u(t)\, dt. \tag{8}$$

In a digital data analysis, the continuous signal is replaced by a digital sample record. Taking T as the total sample time and N the corresponding number of samples, the sampling rate is given by $S_R = N/T = N\,F$.

Thus, the mean value of a finite sample record, $u(j)$, j = 1,2,..., N can be given by

$$\overline{u} = \frac{1}{N}\sum_{j=1}^{N} u(n). \tag{9}$$

The autocorrelation function shown the dependence of the data at one time in relation to the values at another time. An estimate of the autocorrelation function with a time delay $\tau = r/F$ can be written as

$$R_u(r/F) = \frac{1}{N-r}\sum_{j=1}^{N-r}\left[u(j)-\bar{u}\right]\left[u(j+r)-\bar{u}\right], \quad r = 0,1,2,\cdots,m. \tag{10}$$

where r is the lag number and m is the maximum lag number.

The autocorrelation coefficient function is defined by

$$\rho_u(r/F) = \frac{R_u(r/F)}{R_u(0)}. \tag{11}$$

The auto-spectral density function is defined in terms of a Fourier transform of the previously calculated correlation function

$$S_u(f) = \int_{-\infty}^{\infty} R_u(\tau)e^{-i2\pi f\tau}\, d\tau. \tag{12}$$

The auto-spectral density function can also be evaluated from a finite Fourier transform of the data record. Define

$$S_x(f,T,k) = \frac{1}{T}u_k^*(f,T)u_k(f,T), \tag{13}$$

where

$$u_k(f,T) = \int_0^T u_k(t)e^{-i2\pi ft}\, dt. \tag{14}$$

Quantity $u_k(f,T)$ represents a finite Fourier transform of $u_k(t)$ and * denotes the complex conjugate.

Then, $S_u(f)$ can be defined by

$$S_u(f) = \lim_{T\to\infty} E\left[S_x(f,T,k)\right], \tag{15}$$

where $E\left[S_x(f,T,k)\right]$ is the expected value by taking the ensemble average.

Here, the auto-spectrum was estimated by computing an ensemble of estimates from different sub-records. This procedure drastically reduces the auto-spectrum random error.

The corresponding integral time-scale for the autocorrelation function is given by

$$Ti_u = \int_0^{\infty} \rho_u(\tau)d\tau. \tag{16}$$

The integral times scales give a measure of the time separation in which the two fluctuating parameters $u'(t)$ and $u'(t+\tau)$ are correlated with themselves. So that two signals can be considered statistically uncorrelated we must have a time interval between samples of the order of $\tau = 2Ti$.

The second order moments, also called the variance, is given by

$$\sigma_u^2 = \overline{u'\ u'} = \frac{1}{Nn_u - 1}\left\{\sum_{j=1}^{Nn_u}\left[u(j)\right]^2 - Nn_u\ \bar{u}^2\right\} \tag{17}$$

The turbulent intensity is given by

$$Tu = \frac{\sqrt{\overline{u'\ u'}}}{\bar{u}}, \tag{18}$$

The third and forth order moments, also known as the skewness and the kurtosis, or flatness factor, are given by

$$\sigma_u^3 = \overline{(u')^3} = \frac{1}{Nn_u}\left\{\sum_{j=1}^{Nn_u}\left[u(j)\right]^3 - 3\bar{u}\sum_{j=1}^{Nn_u}\left[u(j)\right]^2 + 2\ Nn_u\ \bar{u}^3\right\} \tag{19}$$

and

$$\sigma_u^4 = \frac{1}{Nn_u}\left\{\sum_{j=1}^{Nn_u}\left[u(j)\right]^4 - 4\bar{u}\sum_{j=1}^{Nn_u}\left[u(j)\right]^3 + 6\bar{u}^2\sum_{j=1}^{Nn_u}\left[u(j)\right]^2 - 3\ Nn_u\ \bar{u}^4\right\} \tag{20}$$

The uncertainties (P=99) associated with the measured statistical quantities are given by

$$\bar{u}(\theta) = \bar{u} \pm \frac{2,57}{\sqrt{Nn_u}}\bar{u}\ Tu \tag{21}$$

$$\overline{u'(\theta)\ u'(\theta)} = \overline{u'\ u'} \pm 2,57\frac{\overline{u'\ u'}}{\sqrt{Nn_u}}. \tag{22}$$

$$\overline{u'(\theta)\ u'(\theta)\ u'(\theta)} = \overline{u'\ u'\ u'} \pm 2,57\left(\overline{u'\ u'}\right)^{3/2}\sqrt{\frac{6}{Nn_u}}. \tag{23}$$

$$\overline{u'(\theta)\ u'(\theta)\ u'(\theta)\ u'(\theta)} = \overline{u'\ u'\ u'\ u'} \pm 2,57\left(\overline{u'\ u'}\right)^2\sqrt{\frac{96}{Nn_u}}. \tag{24}$$

4. Small scales

Although the large eddies contribute to most of the transport of momentum and scalars, we know viscous dissipation of turbulence to be determined by the smallest of the eddies.

In this section, we will show how the smallest length scales in a turbulent flow can be found (Tennekes and Lumley (1972)).

Consider that small-scale motions have small time scales, which are statistically independent of the large scales. This argument leads to the conclusion that the rate of energy supply should equal the rate of dissipation. This is basis of Kolmogorov's universal equilibrium theory. This theory suggests that the microscales of length, time and velocity are given by

$$\eta = \left(\frac{\nu^3}{\varepsilon}\right)^{1/4}, \qquad \varphi = \left(\frac{\nu}{\varepsilon}\right)^{1/2}, e \qquad \upsilon = (\nu\varepsilon)^{1/4}. \tag{25}$$

The autocorrelation coefficient defines a further important microscale, Λ_u, which is defined by the curvature of ρ_u at the origin:

$$\left.\frac{d^2\rho_u(\zeta)}{d\zeta^2}\right|_{\zeta=0} = -\frac{2}{\Lambda_u^2} \tag{26}$$

The length scale Λ_u is called the Taylor time microscale; it is directly associated with the dissipation rate in a turbulent flow.

Expanding $\rho_u(\zeta)$ in a Taylor series around the origin, we can write for small values of ζ,

$$\rho_u(\zeta) \cong 1 - \frac{\zeta^2}{\Lambda_u^2}. \tag{27}$$

To correlate the Taylor time microscale with the longitudinal spectrum, we make

$$\overline{\left(\frac{du'}{dt}\right)^2} = 2\frac{\overline{u'u'}}{\Lambda_u^2}. \tag{28}$$

Then, applying Taylor hypothesis to the above equation,

$$\overline{\left(\frac{du'}{dx}\right)^2} = \frac{2}{\bar{u}^2}\frac{\overline{u'u'}}{\Lambda_u^2}. \tag{29}$$

The Taylor length microscale, χ_u, is given by

$$\overline{\left(\frac{du'}{dx}\right)^2} = \frac{\overline{u'u'}}{\chi_u^2}, \tag{30}$$

and the following relation holds

$$\chi_u = \frac{\bar{u}}{\sqrt{2}}\Lambda_u \tag{31}$$

Finally, considering the turbulence isotropic, the dissipation rate, ϵ, can be evaluated from

$$\epsilon = 15\nu\frac{\overline{u'\ u'}}{\chi_u^2}. \tag{32}$$

5. Data reduction

As mentioned in the introduction, the present study resorted to the hot-wire anemometry to measure the properties of the turbulent flow. To accounted for any temperature variation, a temperature-compensated Dantec probe, model 55P76, was used. This probe consists of two sensor elements: a hot-wire and a resistance-wire, usually called cold-wire, situated 2 mm below and 5 mm downstream of the former. Both sensors are Pt-plated tungsten wires, 5 μm in diameter, overall length of 3mm and sensitive wire length of 1,25 mm. They are copper and gold plated at the ends to approximately 30 μm. They were connected respectively to a constant temperature bridge, Dantec 55M10 and to a constant current bridge, Dantec 56C20.

Reference measurements for velocity were obtained from a Pitot tube connected to an inclined manometer; temperature reference data was obtained from previously calibrated micro-thermocouples.

The temperature dependence of the thermal anemometer signal was accounted for by the linear correction method, where the heat transfer from the probe is assumed to be proportional to a product of the temperature difference $T_w - T_a$ and a function of the velocity, where T_w is the temperature of the heated wire and T_a is the ambient temperature. The output voltage, E, of a constant temperature hot-wire anemometer can hence be represented by:

$$E^2 = f(U)(T_w - T_a). \tag{33}$$

Temperature measurements with resistance wires require both low drift, low noise constant current anemometers and high quality amplifiers. If the resistance wire is heated by a current $I = 0.15mA$, then the "hot" resistance R_w will only deviate from R_a by $(R_w - R_a)/R_a \simeq 0.0004$, and the corresponding temperature difference $(T_w - T_a)$ will be less than 0.1 ^oC.

Thus, a common practice is to consider $R_w = R_a$, with

$$R_a = R_0\left[1 + \alpha_0(T_a - T_o)\right]. \tag{34}$$

For practical applications, it is recommended that a temperature calibration of the resistance-wire is used to determine the calibration constants in the relationship

$$R_a = A + B\,T_a. \tag{35}$$

To establish the velocity and temperature sensitivity of the hot-wire probe operating at a fixed hot resistance, R_w, the anemometer output voltage, E_w, was red as a function of the velocity, U, and the fluid temperature, T_a. This type of calibration is often carried out by performing a velocity calibration at a number of different fluid temperatures.

The functional form of the calibration data was then written as

$$E = F(U, T_a - T_w)_{T_w = const}. \tag{36}$$

Equation 36 is a very good approximation to the velocity calibration data, obtained at a constant value of T_a, provided the calibration constants are determined by a least-squares curve fit. This procedure has been applied by other authors to their velocity calibration data using the wire voltage relationship

$$\frac{E_w^2}{R_w\,(R_w - R_a)} = A + BU^n. \tag{37}$$

This curve-fitting procedure gave the most accurate results. When a constant value of $n(= 0.45)$ was selected, A and B also became constants, and the increase in the uncertainty is insignificant for most hot-wire anemometry applications.

The sampling rate was 2500 Hz, and the total measuring time for each point, 53 seconds.

6. Experimental facilities

The low-velocity, stratified-flow, wind tunnel used in this work was described in detail in Cataldi et al.(2001, 2002) and in Loureiro et al. (2001). The tunnel main objective is to simulate stratified atmospheric boundary layers. Some improvements have been recently made in the tunnel to achieve a better representation of atmospheric flows and similarity conditions. The test section has now an overall length of 10 m, with a cross section area of 0.67 m x 0.67 m. The position of the roof is adjustable so as to produce different pressure gradients. The potential velocity of the wind tunnel varies from zero to 3,5 m/s, and the free stream has a turbulence intensity of about 2%.

The stratification section, consisting of 10 electrical resistances, is capable of heating the flow differentially up to 100 ^oC; each of the resistances can be controlled individually. Following the heating section, the floor temperature can also be raised by 100 ^oC over a 6m long surface, by a series of resistances with a controlled variation of 5^oC. The total heating capacity of each panel is about 7 kW/m^2.

The flow was subjected to a step change in roughness (from rough-to-smooth) after traveling the first six meters over a rough wall. The rough surface consisted of roughness elements constructed from equally spaced transversal rectangular slats. The dimensions of the roughness elements were K (= 4.7625 mm), where denotes the height, S (= 15.875 mm) the length, W (= 15.875 mm) the gap, and λ (= 31.75 mm) the pitch. In constructing the surface, extreme care was taken to keep the first roughness element always depressed below the smooth surface, its crest kept aligned with the smooth glass wall surface.

The glass surface was always kept at 25 $^oC \pm 0.5$ ^oC. The next 6 meters, fitted with the rough surfaces, had their temperature raised to 75 $\pm$ 3 ^oC. In fact, the variation in surface temperature for most of the plates was very small, within $\pm$ 1 ^oC. However, the plates were manufactured in such a way that, at the junction (over a length of 10 cm), conjugated effects resulted in a small decrease in temperature ($-$ 3 ^oC). The wall temperature was controlled by 15 thermocouples, set at five stream-wise stations at three span-wise positions.

7. Results

The autocorrelation function, the Kolmogorov length scale and the energy spectra are shown in Figure 1. The evidence is that for measurements taken with a time shift over 0.2 seconds the data were uncorrelated.

The Kolmogorov scales are shown to vary very little with the flow transition regime. Thus, they do not present any significant longitudinal variation. The change in the energy spectra for the flow over a rough surface is noticeable. In particular, in the low frequency region, the energy level is considerably higher for the rough surface flow.

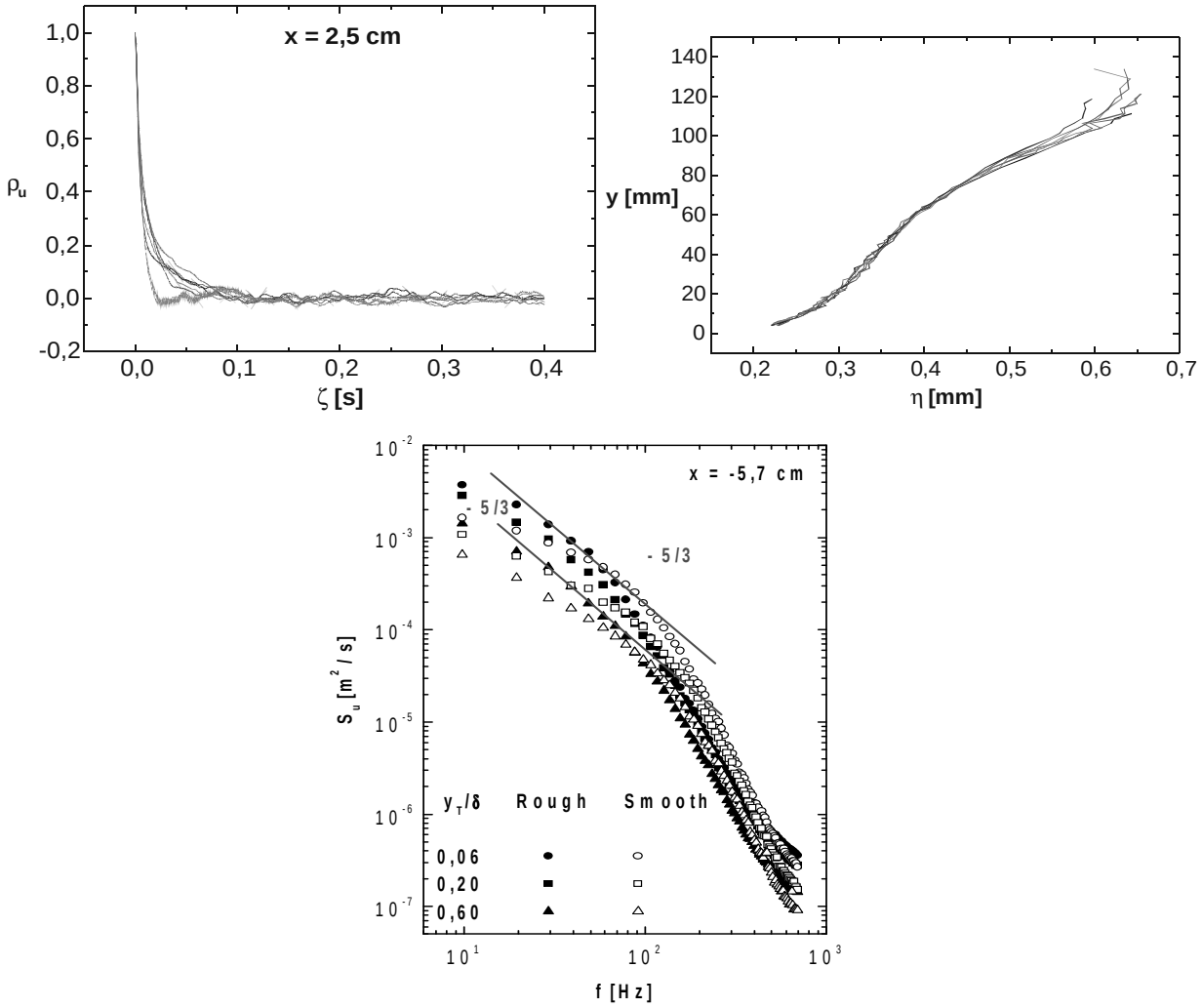

Figure 1: Autocorrelation function, the Kolmogorov length scales and the energy spectra. Curves were drawn for the following stations: x= -6,2, 0.5, 2.5, 5.5, 9.5 and 24.5 cm. The reference x=0 is the point of surface change.

The spectra show clearly an inverse-power-law region where the Kolomogorov scaling can be identified. The -5/3 power law region could be well discriminated, showing the inertial subrange.

The major changes in flow conditions are illustrated by the mean velocity profiles, Figure 2, and by the second-order moments. Note that the flow that leaves the rough wall region in a self-preserving state needs an extra 245 mm of development to reach a new self-preserving state downstream of the transition point. Thus, for all of this transition length, the flow retains part of the properties it had acquired over the rough surface. In particular, so that the slope method of Clauser can be used to evaluate the skin-friction coefficient, the wall turbulent velocity region has to be treated according to the procedure of Perry and Joubert (1963). This will define a "virtual" error in origin for the smooth, flat surface that has to decrease from its largest upstream value soon after the transition point to zero far downstream.

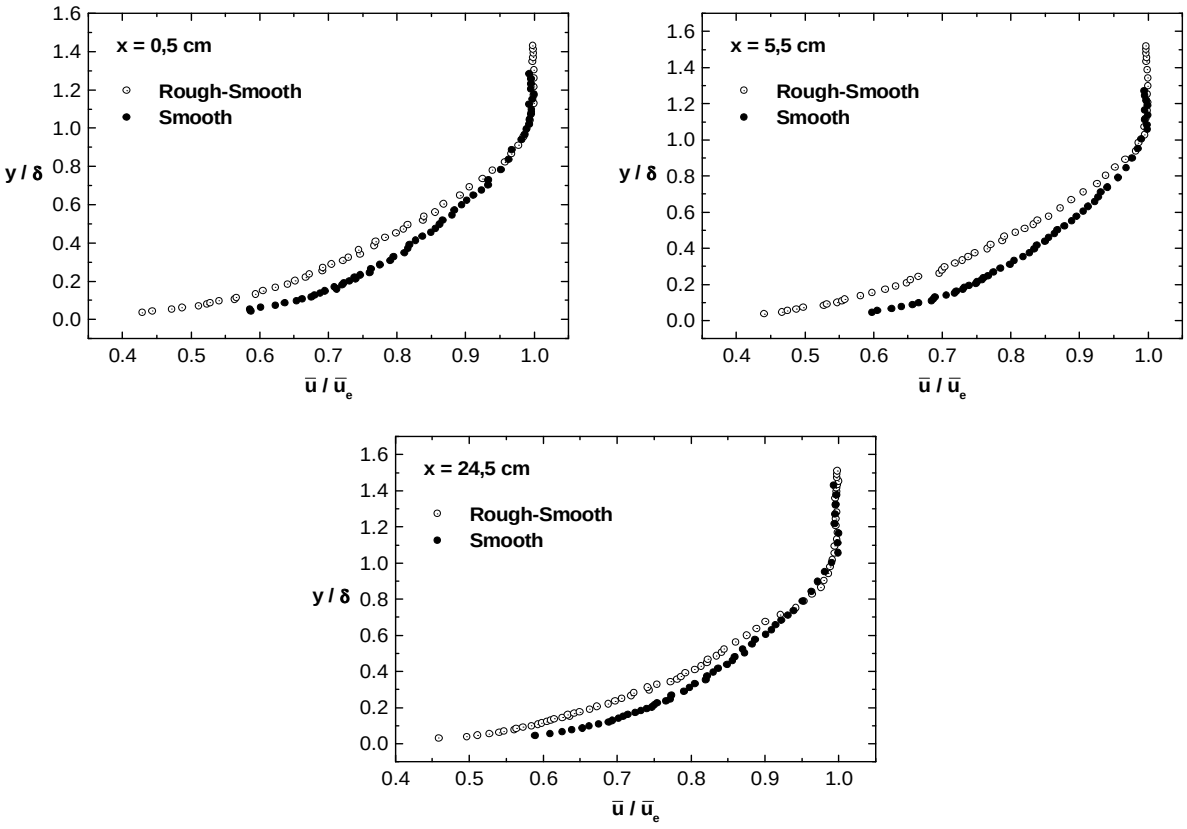

Figure 2: Mean velocity profiles. δ denotes the boundary layer thickness; $\overline{u_e}$ denotes the external flow mean velocity.

The error in origin and the roughness function were found here according to the method of Perry and Joubert (1963). This procedure has been recently reviewed by Avelino and Silva Freire (2002) and thus will not be discussed further here. However, we must note that the error in origin, ε, and the roughness function, Δu, are defined by the equation below where the notation is classical.

$$u^+ = \frac{1}{\kappa} \ln \left[\frac{(y_T + \epsilon)\, u_\tau}{\nu} \right] + A - \frac{\Delta \bar{u}}{u_\tau} \tag{38}$$

The asymptotic behaviour of the error in origin, of the roughness function and of the boundary layer shape factor ($= \delta_1/\delta_2$) are illustrated in Figure 3. These graphs show that about 50 cm are necessary for the boundary layer to adjust back to its undisturbed values.

The second-order moments shown in Figure 4 are particularly affected by the upstream wall condition. For the whole x-wise distance, where the profiles were measured, a non-equilibrium condition was observed. The high turbulence levels originated at the rough wall showed a reasonably slow decay rate.

The third-order moments (Figure 5) are negative in most of the outer region, and positive in the near-wall region. Also, because they are much the same for flows over smooth or rough walls, they tend to collapse onto a single line.

The turbulent kinetic energy dissipation rate is also shown in Figure 5. Of course, ϵ is observed to vary significantly as it departs from the transition region. The dissipation of kinetic energy in the rough wall region must be at its maximum, tending to a lower level in the self-preserving smooth region.

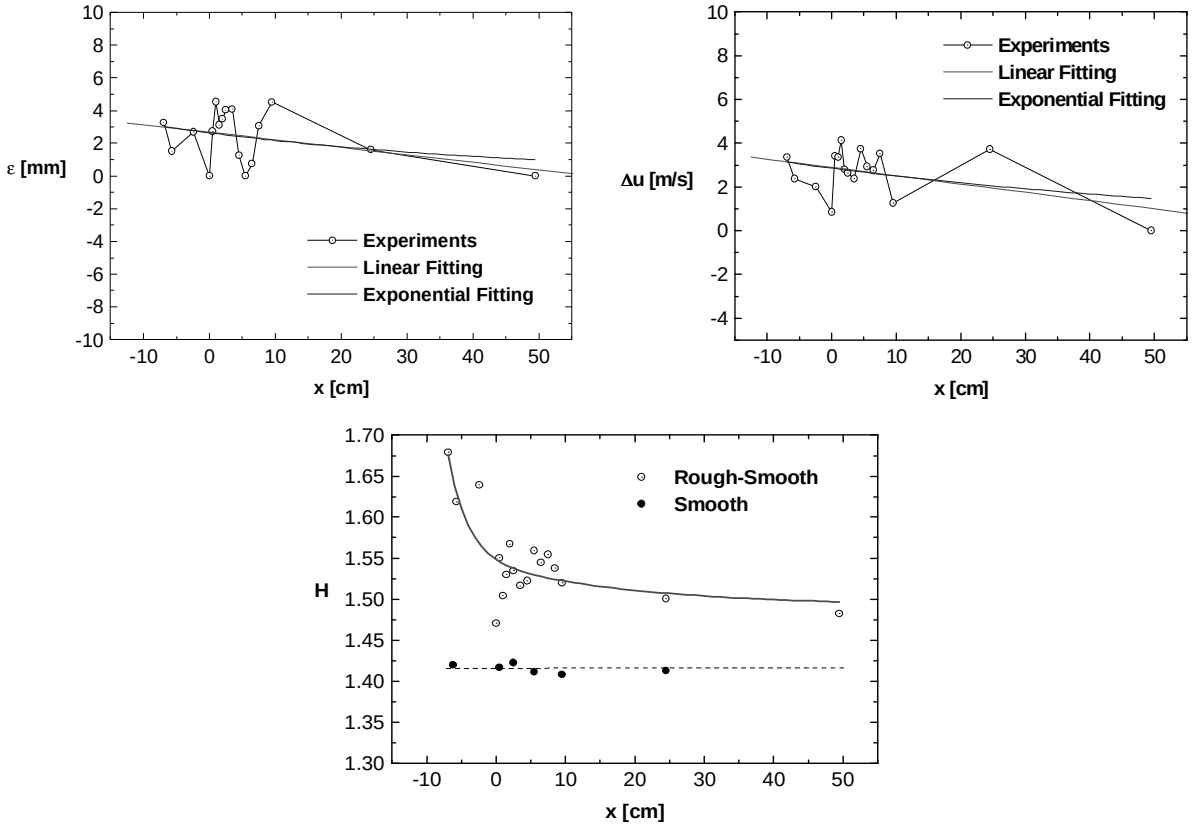

Figure 3: The behaviour of the error in origin and of the roughness function for the rough to smooth transition region.

8. Final Remarks

The data presented in this paper have shown that soon after a change in surface properties, from rough to smooth, some of the statistical characteristics of the flow go through a slow recovery process. That is due to the fact that the rough-wall flow dominates the rate of diffusion of the disturbances for a considerable length, dictating conditions that are not self-preserving. The second-order moments are an example of this occurrence.

On the other hand, the fact that the spectra suffers very little, or even none, influence of the roughness length scale is significant to illustrate that simple turbulence models will not be able to correctly simulate all the flow characteristics. In other words, we have shown that to try to characterize a flow over a rough surface by just modelling the effects that the protuberances have on the mean velocity or temperature profiles is simply not enough, more sophisticated models are needed.

In any case, the present characterization of the transition region, from rough to smooth, is thought to be detailed enough to provide the necessary data for a careful assessment of any proposed turbulent model that is supposed to describe the problem.

Acknowledgments. The present work has been financially supported by the Brazilian National Research Council, CNPq (Grant No 472215/2003-5), and by the Rio de Janeiro Research Foundation, FAPERJ, through the PRONEX Grant No E-26/171.198/2003, in the context of the Nucleus of Excellence in Turbulence. APSF is grateful to the CNPq for the award of a Research Fellowship (Grant No 304919/2003-9). APSF further benefited from a Research Fellowship from FAPERJ (E-26/152.368/2002).

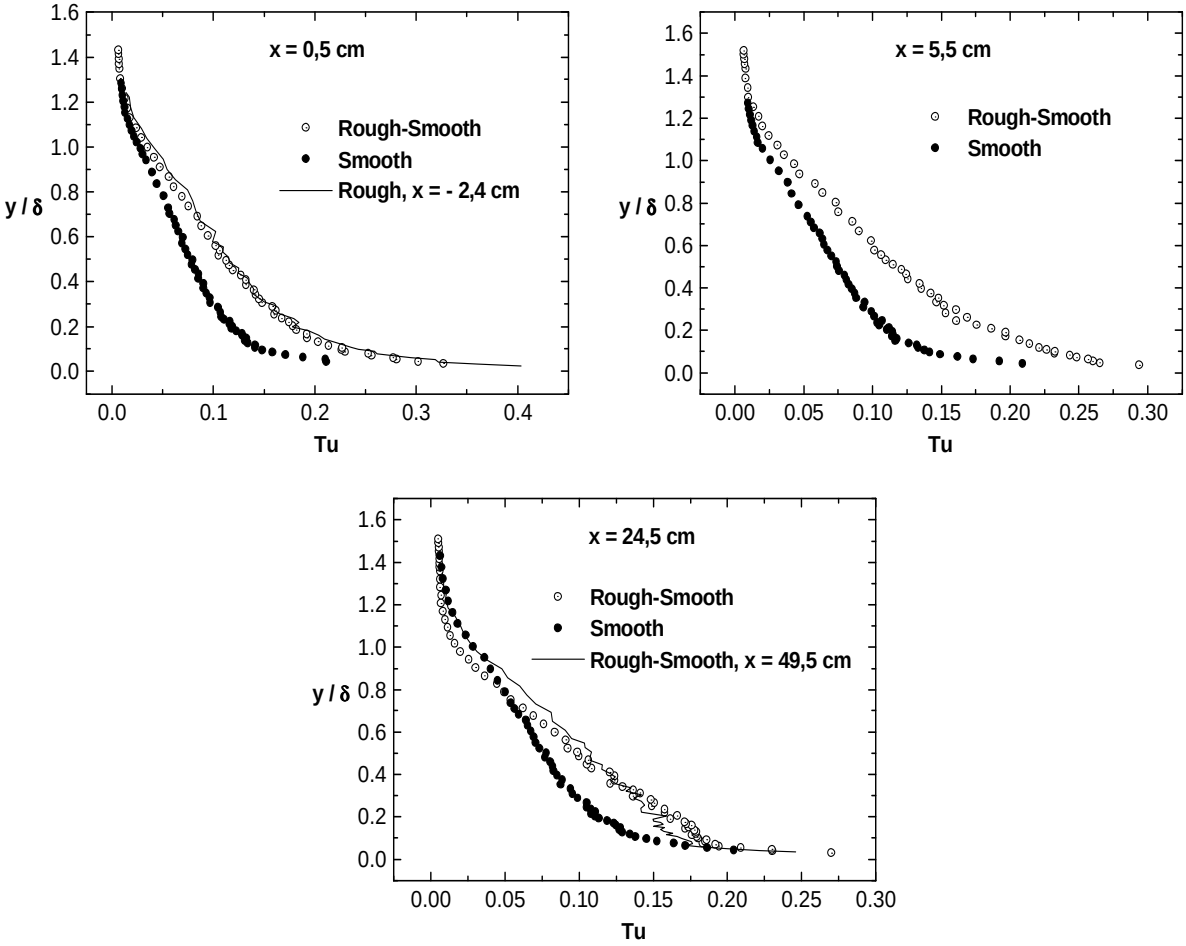

Figure 4: Longitudinal turbulent intensity.

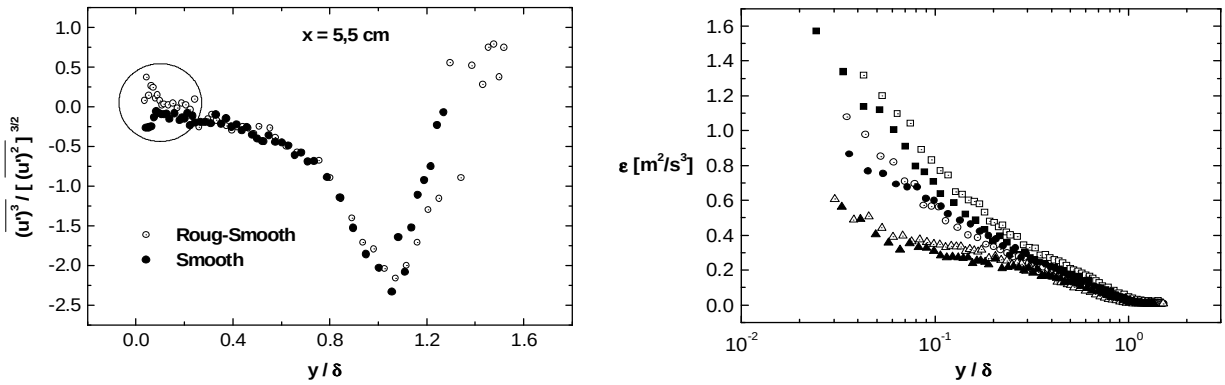

Figure 5: Longitudinal third-order moments and the turbulent kinetic energy dissipation rate. Curves were drawn for the following stations: x= -6,2, 0.5, 2.5, 5.5, 9.5 and 24.5 cm. The reference x=0 is the point of surface change.

9. References

Avelino, M. R. and Silva Freire, A. P., 2002, On the displacement in origin for turbulent boundary layers subjected to sudden changes in wall temperature and roughness, Int. J. Heat and Mass Transfer, 45, 3145-3153.

Antonia, R.A. and Luxton, R.E., 1971, The response of a turbulent boundary layer to a step change in surface roughness. Part 1. Smooth to Rough, J. Fluid Mechanics, 48, 721–761.

Antonia, R.A. and Luxton, R.E., 1972,The Response of a Turbulent Boundary Layer to a Step Change in Surface Roughness Part 2. Rough to Smooth, J. Fluid Mechanics, 53, 737–757.

Antonia, R.A., Danh, W.H. and Prabhu, A., 1977, Response of a Turbulent Boundary Layer to a Step Change in Surface Heat Flux, J. Fluid Mechanics, 80, 153-177.

Bandyopadhyay, P.R., 1987, Rough Wall Turbulent Boundary Layers in the Transition Regime, J. Fluid Mechanics, 180, 231-266.

Bandyopadhyay, P.R. and Watson, R. D., 1988, Structure of rough-wall turbulent boundary layers, Phys. Fluids, 31, 1877-1883.

Bruun, H. H., 1995, Hot-wire Anemometry - Principles and Signal Analysis, Oxford University Press.

Cataldi, M., Loureiro, J. B. R., Pimentel, L. C. G. e Silva Freire, A. P., 2001, Design features and flow measurements in a thermally stratified wind tunnel", XVI Congresso Brasileiro de Engenharia Mecânica (COBEM), Uberlândia.

Cataldi, M., Loureiro, J. B. R., Pimentel, L. C. G. e Silva Freire, A. P., 2002, A comparison between wind tunnel simulation and field measurements of the atmospheric boundary layer", Anais do IX Congresso Brasileiro de Engenharia e Ciências Térmicas (ENCIT), Caxambu.

Krogstad, P.-A. and Antonia, R. A., 1994, Structure of turbulent boundary layers on smooth and rough walls, J. Fluid Mechanics, 277, 1-21.

Loureiro, J. B. R., Cataldi, M. e Silva Freire, A. P., 2001, An experimental study of turbulent stratified flows over hills with large changes in surface elevation", XVI Congresso Brasileiro de Engenharia Mecânica (COBEM), Uberlândia, dezembro.

Perry, A.E., and Joubert, P.N., 1963, Rough Wall Boundary Layers in Adverse Pressure Gradients, J. Fluid Mechanics, 17, 193–211.

Perry, A.E., Lim, K.L. and Henbest, S.M., 1987, An Experimental Study of the Turbulence Structure in Smooth- and Rough-Wall Boundary Layers, J. Fluid Mechanics, 177, 437–466.

Tennekes, H. And Lumley, J. L., 1972, A first course in turbulence, MIT Press.

P.M. Ligrani and R.J. Moffat, 1985, Thermal Boundary Layers on a Rough Surface Downstream of Steps in Wall Temperature, Boundary Layer Meteorology, 31, 127-147.